

Adhesion of fluid vesicles at chemically structured substrates

G.T. Linke, R. Lipowsky, and T. Gruhn^a

Max Planck Institute of Colloids and Interfaces, Science Park Golm, D-14424 Potsdam, Germany

Received 16 January 2007 and Received in final form 1 June 2007

Published online: 29 November 2007 – © EDP Sciences / Società Italiana di Fisica / Springer-Verlag 2007

Abstract. The adhesion of fluid vesicles at chemically structured substrates is studied theoretically via Monte Carlo simulations. The substrate surface is planar and repels the vesicle membrane apart from a single surface domain γ , which strongly attracts this membrane. If the vesicle is larger than the attractive γ domain, the spreading of the vesicle onto the substrate is restricted by the size of this surface domain. Once the contact line of the adhering vesicle has reached the boundaries of the γ domain, further deflation of the vesicle leads to a regime of low membrane tension with pronounced shape fluctuations, which are now governed by the bending rigidity. For a circular γ domain and a small bending rigidity, the membrane oscillates strongly around an average spherical cap shape. If such a vesicle is deflated, the contact area increases or decreases with increasing osmotic pressure, depending on the relative size of the vesicle and the circular γ domain. The lateral localization of the vesicle's center of mass by such a domain is optimal for a certain domain radius, which is found to be rather independent of adhesion strength and bending rigidity. For vesicles adhering to stripe-shaped surface domains, the width of the contact area perpendicular to the stripe varies nonmonotonically with the adhesion strength.

PACS. 87.16.Dg Membranes, bilayers, and vesicles – 68.15.+e Liquid thin films – 87.16.Ac Theory and modeling; computer simulation

1 Introduction

In the last decade, a growing number of applications for fluid vesicles has been developed. One important application area are vesicles as components in microtechnological systems. Vesicles can be used, for example, as microcompartments for the investigation of chemical reactions [1], as modules of membrane sensors [2,3], and as basic building blocks of complex membrane networks [4]. In most of these applications, the vesicles have to be spatially immobilized, and so they are typically attached to a substrate. In order to localize the vesicle within the substrate surface plane, one may use an attractive circular domain within a chemically heterogeneous substrate. In a further step, adhesive stripes may be used to elongate the adhering vesicle or to specify pathways along which the adhering vesicle can be moved by an external force.

Vesicle adhesion on chemically structured substrates has been investigated for various widths of the attractive domains. In many cases, the extensions of the attractive patches are distinctly larger than the vesicle diameter. Depending on the adhesion strength the adhering vesicles may either stay intact or they may rupture and fuse with adjacent vesicles, forming a lipid bilayer that covers the area of the attractive patch [5]. In this way, a set of lipid

bilayer stripes can be created. If suitable proteins or ligands are included in the membranes, the stripes can be used for cell recognition or to test the adhesion strengths to receptor-covered beads [6,7]. In another experiment, the width of the adhesive stripes was chosen distinctly smaller than the diameter of the adhering giant vesicle [8]. As the vesicle adheres to the substrate, the stripes generate strong local membrane deformations and permeations which again disappear after one or two minutes.

If the attractive domains are used to localize the vesicles, the diameter of the domains is comparable or slightly smaller than that of the vesicle. Examples are vesicles linked by lipid nanotubes to serve as reactors in a chemical nano-laboratory. Circular attractive domains have been used to localize the vesicles which were linked by the sometimes rather complex network of lipid nanotubes [4]. Arrays of isolated vesicles and cells are of great relevance for biosensors since they combine a large detection area with the facility to discern single biomolecule reactions (compare with Refs. [9,10]). In order to avoid interference or fusion of neighboring vesicles, the attractive patches or stripes must be separated by sufficiently large distances. One scope of this article is to determine the lateral extension and the range of lateral fluctuations for vesicles adhering to an attractive substrate region.

Equilibrium shapes of free vesicles and vesicles which adhere to a homogeneous substrate have been studied

^a e-mail: gruhn@mpikg.mpg.de

analytically by several groups. Shape equations for axially symmetric vesicles have been derived and numerically solved in the early nineties of the last century [11, 12]. Some years later, analytic expressions for the shape of axisymmetric adhering vesicles were derived for the case of low bending rigidity [13, 14]. Some general properties of the adhesion zone boundary were found for non-symmetrical vesicles adhering to not necessarily planar substrates [15]. Dynamical aspects of vesicle adhesion have been investigated experimentally and analytically for homogeneously binding vesicles and vesicles with mobile sticker molecules [16–18]. Further analytic studies were made for the force-induced unbinding of vesicles [19, 20] and the lateral motion of vesicles occurring under certain conditions [21, 22]. At finite temperature, thermal fluctuations are typically of great relevance. As recently shown for free vesicles, thermal fluctuations can infer qualitative changes of the vesicle morphology [23]. The influence of thermal fluctuations on vesicles which adhere to a homogeneous substrate has been studied with analytical [24] and simulation methods [25–27].

In this article, we investigate properties of vesicles adhering to a chemically heterogeneous substrate. We assume that the substrate has two types of surface domains, γ and δ , which attract and repel the vesicle, respectively. In the following, we are interested in substrates with attractive domains whose characteristic lengths are comparable with the vesicle diameter. Properties of the equilibrium shape of vesicles on finite domains have been presented in an article in 2005, together with a description of related experiments [28]. However, influences of thermal fluctuations on the morphology of these vesicles have neither been studied theoretically nor experimentally in detail. In this article, we give an insight into fluctuation-based phenomena and provide results relevant for the localization and controlled deformation of adhering vesicles.

In the absence of fluctuations, the shape of a vesicle adhering to a finite attractive patch has been shown to be intimately related to the shape of a liquid droplet wetting the same surface patch [28]. Since the energy functional for the shape of an adhering vesicle is similar to that of a liquid droplet on a substrate except for the bending energy and the constant surface area, the shapes that minimize the energy functional of an adhering vesicle with small bending rigidity and those of droplets show similar properties. Therefore, adhering vesicles with relatively low bending rigidity or relatively large membrane tension are predicted to behave very similar to adhering liquid droplets, if thermal fluctuations are negligible. In this article, we use Monte Carlo simulations and a simple analytic approach to explore the relation between the wetting behavior of liquid droplets and the adhesion of strongly fluctuating vesicles.

The article is organized as follows. After a description of the model system in Section 2, we report results from Monte Carlo simulations for a fluid vesicle that adheres to a planar substrate with a circular γ domain in Section 3. In this context, we investigate how strongly the vesicle is localized laterally on this attractive domain. In Section 4,

we present the results of similar simulations for a vesicle on a striped γ domain within the substrate.

2 The model system

We are interested in the properties of the surface shape S_{ve} of an adhering vesicle which is considered to have a fixed area $A = 4\pi R_0^2$. The vesicle membrane can perform fluctuations on roughly all length scales between the vesicle diameter and the thickness of the membrane. In the simplest case, the elastic bending energy can be written as [29, 30]

$$E_{el} = 2\kappa \oint_{S_{ve}} dA M^2, \quad (1)$$

where κ is the bending rigidity and M is the mean curvature. Typically, vesicles used in microtechnology have diameters of the order of $10 \mu\text{m}$ [1, 3, 4] and a bending rigidity of the order of $\kappa \simeq 10 T$, where the Boltzmann constant k_B is absorbed into the temperature T . The vesicle volume can change, in principle. It can be stabilized by *osmotically active* particles in- and outside the vesicle, which cannot permeate the lipid membrane. These molecules, which are for instance sugar molecules, have an osmotic impact on the vesicle volume \mathcal{V} which involves the energy contribution

$$E_{osm} = T \left(-N \ln \frac{\mathcal{V}}{\mathcal{V}_{ref}} + c_{ex} \mathcal{V} \right) \quad (2)$$

to the configurational energy. Here, N is the number of osmotically active particles inside the vesicle, \mathcal{V}_{ref} is a reference volume, and c_{ex} is the concentration of osmotically active particles outside the vesicle. In the following, c_{ex} will simply be called the *exterior concentration*. If the vesicle is attached to a homogeneous attractive substrate surface along the xy -plane the adhesion energy is given by

$$E_{ad} = \oint_{S_{ve}} dA V(z), \quad (3)$$

where $V(z)$ is the attractive substrate potential per membrane area. In the following, the membrane-substrate interaction is modelled by a 9-3-Lennard-Jones potential $V_{LJ}(z)$. It has the functional form

$$V(z) = V_{LJ}(z) \simeq W_{LJ} \left(\frac{1}{90} \left(\frac{\sigma_{LJ}}{z} \right)^9 - \frac{1}{12} \left(\frac{\sigma_{LJ}}{z} \right)^3 \right). \quad (4)$$

The strength of the potential per unit membrane area is given by W_{LJ} , while σ_{LJ} is the characteristic range of the potential. The maximum adhesion strength,

$$W_{max} \equiv -\min_{z>0} (V(z)) = \frac{\sqrt{10}}{36} W_{LJ}, \quad (5)$$

is attained for separation $z = z_{max} \equiv (2/5)^{1/6} \sigma_{LJ}$ between membrane and substrate. The Lennard-Jones potential was chosen because it is smooth, short-ranged and

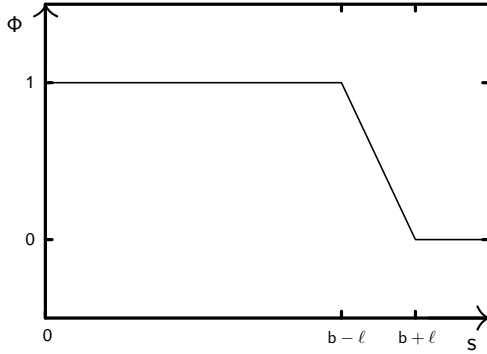


Fig. 1. Schematic plot of the weighting function $\Phi(s, b)$ where ℓ is the mean tether length in the tethered-beads model, $2b$ is the diameter of the attractive domain and s is the distance from the center of the domain.

computationally rather inexpensive even if integrated over the surface of the model vesicle. Apart from these aspects, V_{LJ} serves as a simple generic model potential, representing typical attractive short-range interaction. Especially, if the adhesion strength is large and most parts of the adhering membrane are located close to the potential minimum, V_{LJ} is approximately harmonic like most other potentials. Properties of vesicles adhering to a substrate via V_{LJ} are also comparable with those found for a square-well potential. For both potentials we compared the adhesion behavior of a vesicle with $\kappa = 10T$ attached to a homogenous substrate. Results for the 9-3-Lennard-Jones potential with $\sigma = 0.03$ and those for a square-well potential with a potential depth of W_{max} and a well width of $\sigma/2$ showed good agreement over the whole range of adhesion strengths used in this article.

We consider a hard repulsive interaction at $z = 0$ together with an attractive interaction that is restricted to a finite domain on the substrate, which is either a circle or a stripe. A continuous transition zone between the attractive γ domain and the repulsive δ region is achieved with the help of the continuous function

$$\begin{aligned} \Phi(s, b) &= 1, & \text{for } s < b - \ell, \\ &= \frac{b + \ell - s}{2\ell}, & \text{for } b - \ell \leq s < b + \ell, \\ &= 0, & \text{for } s \geq b + \ell, \end{aligned} \quad (6)$$

where s is the distance from the center of the γ domain, $2b$ is the domain diameter and ℓ is the mean edge length of the used vesicle triangulation, as described below. The function $\Phi(s, b)$, which is shown in Figure 1, is used as a weighting function for the adhesion energy of a circular γ domain with radius R_γ . The latter energy is now obtained via

$$E_{ad}^c = \oint_{S_{ve}} dA \Phi(r, R_\gamma) V(z), \quad (7)$$

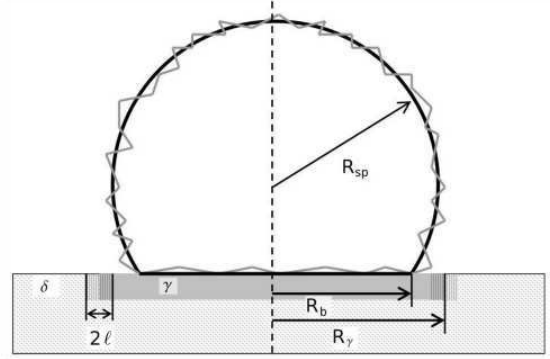


Fig. 2. Geometry of a vesicle adhering to an attractive circular γ domain (grey bar) of radius R_γ , surrounded by a repulsive δ domain (dotted region). Adhering vesicles with low bending rigidity (irregular grey line) fluctuate around a spherical cap geometry characterized by the spherical radius R_{sp} and the circular base radius R_b .

with $r = \sqrt{x^2 + y^2}$, see Figure 2. Correspondingly, the adhesion energy of a γ stripe with width L_γ is defined as

$$E_{ad}^s = \oint_{S_{ve}} dA \Phi(x, L_\gamma/2) V(z). \quad (8)$$

In the simulations the vesicle is represented by a triangulated surface, including $N_t = 996$ triangles. For each triangle, we have used the coordinates x_t and y_t of its center of mass to weight the adhesion energy of the triangle with $\Phi(\sqrt{x_t^2 + y_t^2}, R_\gamma)$ and $\Phi(x_t, L_\gamma/2)$ for the circular and the striped domain, respectively.

The geometry of the model surface is well defined by the coordinates of the vertices and a list that indexes which vertices are connected by edges. In our simulation, the tethered beads model ensures that the distance between any pair of beads is larger than $d \simeq R_0/16$ while vertices connected by an edge stay closer than $\sqrt{3}d$. In each Monte Carlo (MC) move, pseudo-random numbers are used to alter the existing configuration. If this leads to an increase of the energy $\Delta E > 0$, the new configuration is rejected in favor of the old one with a probability $1 - \exp(-\Delta E/T)$, as originally introduced by Metropolis and coworkers [31]. Configurations are altered by two different types of MC moves, which are chosen in random order: In the displacement move the position of one vertex is changed by a small random vector. In the bond-flip move [32], the shared edge of two neighboring triangles is removed and the previously unconnected vertices are connected. Simulations typically consisted of $10^7 N_t$ equilibration moves and the same number of moves to calculate averages.

The simulations were performed with $\kappa = 0.1-20T$. For the short-ranged attractive potential in the γ domain we used $\sigma_{LJ} = 0.03 R_0$.

The influence of osmotically active particles is incorporated by equation (2) which avoids to simulate the individual particles. We choose $N = 10^4$ osmotically active

particles inside the vesicle and an exterior concentration c_{ex} with $2600 \leq c_{ex}R_0^3 \leq 4000$ in the surrounding medium. These values reflect the conditions in experiments with typical concentrations $c = 10^{-4} \text{ mol m}^{-3}$ of osmotically active particles and corresponds to $c\mathcal{V}T \simeq 10^3 \kappa$.

One important quantity that characterizes the geometry of an adhering vesicle is its contact area A^* , which is the size of the membrane region which adheres to the substrate.

For a triangulated vesicle, we found that A^* can be well approximated by the sum of the areas of all triangles that contribute a negative energy less than $-T$ to E_{ad} . This definition is well suited for values $W_{LJ} \gtrsim 2000 T/R_0^2$, corresponding to total adhesion energies $E_{ad} \lesssim -50 T$ and maximum adhesion strengths $W_{max} \gtrsim 175 T/R_0^2 \simeq 17.5\kappa/R_0^2$ for $\kappa = 10 T$. However, for distinctly lower values of W_{LJ} the minimum adhesion energy per triangle, which is $-1.4 \times 10^{-3} W_{LJ}$, gets comparable with the threshold value $-T$. As a consequence, the adhesion area undergoes strong fluctuations and drifts for $W_{LJ} \lesssim 2000 T/R_0^2$ and our definition of A^* gets inadequate for $W_{LJ} \lesssim 1000 T/R_0^2$. Therefore we have restricted simulations to values $W_{LJ} \geq 2000 T/R_0^2$, with one exception in Figure 6b, where reliable results were obtained for $W_{LJ} = 1500 T/R_0^2$ by averaging over $3 \times 10^7 N_t$ Monte Carlo moves.

3 Adhesion to an attractive circular domain

Influence of bending rigidity

We consider a vesicle adhering to a circular adhesive γ domain on an otherwise repulsive substrate. If the vesicle is located at the center of the domain and the domain radius is sufficiently large, the vesicle behaves in the same way as on a homogenous, attractive substrate.

Depending on the bending rigidity of the vesicle, different regimes can be distinguished. The strong adhesion regime is characterized by $|E_{ad}| \gg E_{el}$ such that energy contributions from membrane curvatures are negligible [11, 28]. In this case, the vesicle tends to maximize the adhesion area A^* . For an approximately fixed membrane area A this leads to a minimization of the non-adhering membrane area $A_{na} \equiv A - A^*$. At finite temperature, the shape is subject to small thermal fluctuations, which are smoothed by the membrane tension that is induced by the adhesion.

If the external concentration is increased, the vesicle volume decreases and the adhesion area A^* gets larger. If the vesicle volume \mathcal{V} is continually decreased and the γ domain is smaller than $A/2$, the adhesion area A^* eventually covers the whole γ domain. At a further decrease of \mathcal{V} , the vesicle does not gain more adhesion energy by increasing the adhesion area. As discussed in [28], a further decrease of \mathcal{V} should leave A^* unchanged while the membrane tension decreases. In the appendix, the latter scenario is studied using a simple analytic model. The latter model predicts that the vesicle membrane fluctuates strongly around an average surface with spherical-cap geometry.

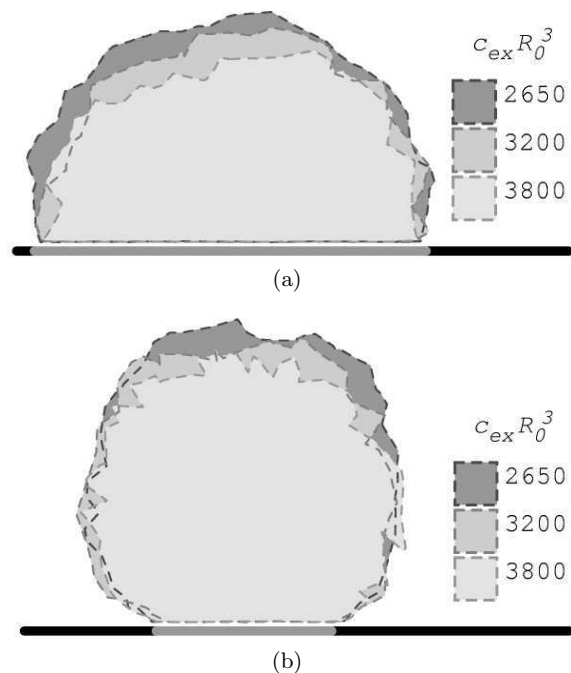


Fig. 3. Typical configurations of a fluid vesicle with bending rigidity $\kappa = 0.1T$ that is adhering to an attractive circular γ domain (gray bar segment) surrounded by a repulsive δ domain (black bar segments). The γ domain has potential strength $W_{LJ} = 5000 T/R_0^2$ and radius (a) $R_\gamma = 1.1 R_0$ or (b) $R_\gamma = 0.5 R_0$. The length R_0 is defined via the vesicle surface area $A = 4\pi R_0^2$. Inside the vesicle, there are $N = 10^4$ osmotically active particles. Configurations for different concentrations c_{ex} of osmotically active particles outside the vesicle are visualized by vertical cuts through the vesicles' center of mass. The contours of the vesicles are plotted on top of the shaded areas that resemble the vesicles' interior.

Thus, in the limit of low bending rigidity, the *average* shape of the fluctuating vesicle is found to approach the surface shape of a liquid droplet. For lipid membranes, the bending rigidity is of the order of $\kappa \simeq 10T$ or larger (see, e.g., [33]), and the fluctuations are essentially reduced. Other surfactants may form membranes with distinctly lower bending rigidities. For example, a mixture of cetyltrimethylammonium tosylate and sodium dodecylbenzene sulfonate (CTAT : SDBS) in a sodium chloride brine has recently been found to form unilamellar vesicles [34]. Measurements of the bending rigidity revealed extremely low values between $\kappa \simeq 0.01T$ and $\kappa \simeq 0.62T$, depending on the CTAT : SDBS composition and the salt concentration.

In the following, the deflation of vesicles, adhering to a finite circular γ domain, is discussed in more detail. First, simulations were performed for a very low bending rigidity $\kappa = 0.1T$. The vesicle volume was determined by the osmotic conditions as described in the previous section. For comparison, a second series of simulations was run with $\kappa = 10T$.

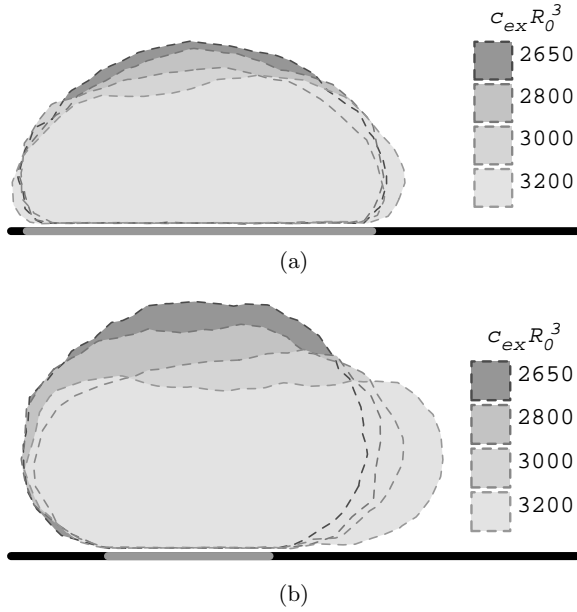


Fig. 4. Typical configurations of a vesicle with bending rigidity $\kappa = 10T$ for the same geometry as in Figure 3.

Typical configurations of a vesicle with $\kappa = 0.1T$ are shown in Figure 3 for a large and a small domain radius and different exterior concentrations c_{ex} . As predicted in [28], they reveal strong membrane fluctuations. By averaging over the small-wavelength deflections, we find the result predicted by the approach in the appendix: The membrane fluctuates around an average shape which is approximately a spherical cap.

The amplitudes of the fluctuations increase with the area difference $A_{na} - A_{av}$ between A_{na} and the area of the average shape A_{av} of the non-adhering membrane. Thus, the membrane fluctuates around the smallest possible surface for a given volume \mathcal{V} with a circular base area, which is a spherical cap.

Altogether we notice:

- A vesicle which is adhering to a sufficiently large and sufficiently attractive domain is in a high-tension regime where the membrane forms a spherical cap in order to maximize the adhesion area.
- If a vesicle is adhering to a sufficiently small, attractive, circular domain, deflation leads to a low-tension regime; with a sufficiently low bending rigidity of the membrane, the average shape of the fluctuating membrane becomes a spherical cap in order to maximize the membrane fluctuations.

Figure 4 shows vesicle shapes for the same conditions as in Figure 3 but for $\kappa = 10T$. The surface is much smoother than for $\kappa = 0.1$, but the average shape of the vesicle deviates distinctly from the spherical cap: The height to width ratio is smaller and there is a smooth transition from the flat adhering to the non-adhering part.

For a more quantitative analysis we fitted the center \mathbf{r}_c and the radius R_{sp} of a sphere, cut at the substrate area,

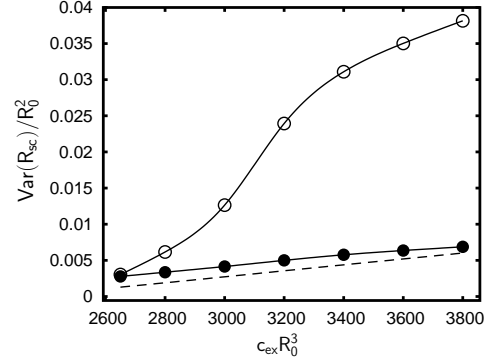


Fig. 5. Reduced squared deviation $\text{Var}(R_{sp})/R_0^2$ from the spherical-cap geometry as a function of the reduced concentration $c_{ex}R_0^3$ of osmotically active molecules outside the vesicle. The reference length R_0 is defined via the vesicle surface area $A = 4\pi R_0^2$. Inside the vesicle there are $N = 10^4$ osmotically active particles. Results are shown for bending rigidity $\kappa = 10T$ (○) and $\kappa = 0.1T$ (●). The dashed line shows results of the analytic approach, discussed in the appendix. Solid lines are intended to guide the eye.

with the non-adhering part of the vesicle configurations. Therefore, only the N_{na} non-adhering vertices \mathbf{r}_i of the triangulated vesicle were considered for the minimization of

$$\text{Var}(R_{sp}) \equiv \frac{1}{N_{na}} \sum_{i=1}^{N_{na}} (\|\mathbf{r}_i - \mathbf{r}_c\| - R_{sp})^2, \quad (9)$$

which vanishes for vesicle configurations with a perfect spherical-cap geometry. As shown in Figure 5, the deviation from the spherical cap increases strongly with the exterior concentration c_{ex} for $\kappa = 10T$. In contrast, vesicles with a low bending rigidity $\kappa = 0.1T$ can be fitted well by a spherical cap over the whole concentration regime as studied here. The dashed line shows results based on the model system in the appendix for a bending rigidity $\kappa = 0.1T$ and a maximum wave number $(2l)^{-1}$. The values as obtained from the model are slightly lower than the corresponding simulation results. In the following, we use R_{sp} for the spherical radius and R_b for the circular base area of the spherical cap. The whole geometry is shown in Figure 2. Values of πR_b^2 were found to agree well with the separately measured projected contact area.

In Figure 6, the average size A_p^* of the projected contact area is shown as a function of the potential strength W_{LJ} of the attractive domain for different osmotic conditions. As expected, A_p^* increases monotonically with W_{LJ} . An increase of the exterior concentration c_{ex} leads to a decrease of the average vesicle volume. Such a decrease of the volume may have two consequences: On the one hand, the surface area of the average spherical-cap geometry may shrink, giving rise to stronger membrane fluctuations and a higher entropy. On the other hand, the base area of the average spherical cap can get larger so that the adhesion energy gets more negative. As a consequence, the behavior of the average projected area A_p^* of a vesicle adhering to a circular domain changes qualitatively with the size of

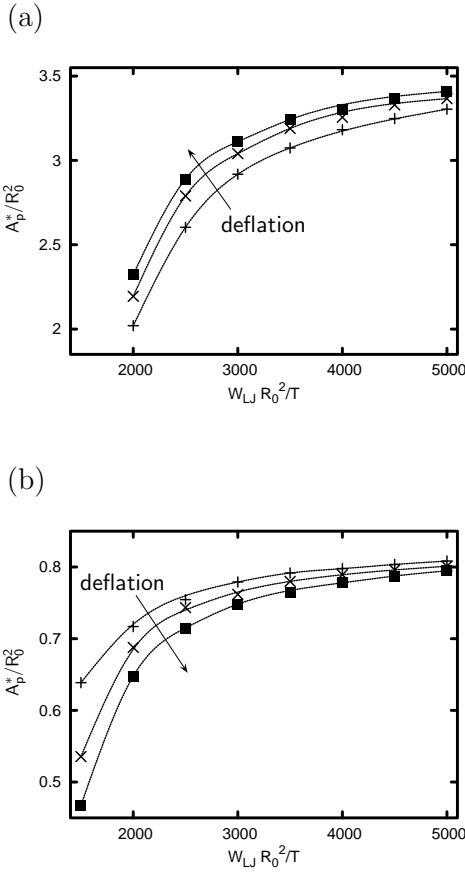


Fig. 6. Reduced projected contact area A_p^*/R_0^2 as a function of the reduced adhesion potential strength $W_{LJ} R_0^2/T$ with a bending rigidity $\kappa = 0.1 T$. The length R_0 is defined via the vesicle surface area $A = 4\pi R_0^2$. Lines are intended to guide the eye. (a) For a circular γ domain with $R_\gamma = 1.1 R_0$, the projected contact area A_p^* increases as the vesicle is deflated, *i.e.* with increasing exterior concentrations $c_{ex} = 2650/R_0^3$ (+), $c_{ex} = 3200/R_0^3$ (x), and $c_{ex} = 3800/R_0^3$ (■). (b) For $R_\gamma = 0.5 R_0$, the projected area decreases under deflation.

the domain radius R_γ . For $R_\gamma = 1.1 R_0$ the average size A_p^* of the projected contact area increases with increasing exterior concentration c_{ex} , *i.e.* deflating volume, while for $R_\gamma = 0.5 R_0$ the size of A_p^* decreases with increasing c_{ex} for all attraction strengths. For a large radius of the attractive domain, the reduction of the volume allows the vesicle to increase the projected contact area so that the remaining γ domain is covered. For the small radius R_γ the attractive domain is essentially covered with the adhering membrane even for the largest vesicle volume, found with the exterior concentration $c_{ex} = 2650 R_0^{-3}$. If c_{ex} is increased, the vesicle volume decreases and promotes fluctuations of the membrane which on average turn out to reduce the projected contact area.

A corresponding effect can be observed for the radius R_{sp} of the average spherical cap as a function of the domain radius R_γ , as shown in Figure 7(a) for $W_{LJ} =$

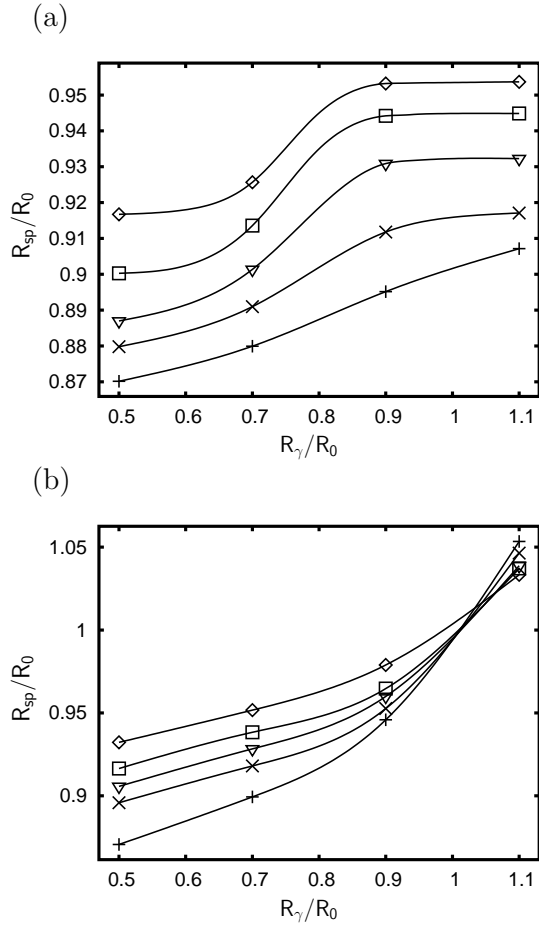


Fig. 7. Reduced spherical radius R_{sp}/R_0 of a spherical cap fitted to a vesicle with bending rigidity $\kappa = 0.1 T$ that is adhering to an attractive domain with radius R_γ . The length R_0 is defined via the vesicle surface area $A = 4\pi R_0^2$. Results are shown for adhesion potential strengths $W_{LJ} = 2000 T/R_0^2$ (a) and $W_{LJ} = 4000 T/R_0^2$ (b), and for exterior concentrations $c_{ex} = 2800/R_0^3$ (◇), $c_{ex} = 3000/R_0^3$ (□), $c_{ex} = 3200/R_0^3$ (▽), $c_{ex} = 3400/R_0^3$ (x), and $c_{ex} = 3600/R_0^3$ (+). Lines are intended to guide the eye.

$2000 T/R_0^2$ and in Figure 7(b) for $W_{LJ} = 4000 T/R_0^2$. Results are presented for various values of c_{ex} . For small domain radii R_γ , vesicles exposed to smaller c_{ex} and correspondingly larger volume are more inflated and have a larger spherical radius R_{sp} than vesicles with a smaller volume. For $W_{LJ} = 2000 T/R_0^2$ the radius of R_{sp} increases with increasing R_γ up to $R_\gamma \approx 0.9 R_0$ where vesicles exposed to lower exterior concentration $c_{ex} \leq 3200 R_0^{-3}$ reach a plateau, while vesicles exposed to larger c_{ex} continue to increase. Apparently, for $W_{LJ} = 2000 T/R_0^2$ the larger vesicles have an optimum adhesion area corresponding to the size of the γ domain with a radius $R_\gamma \approx 0.9 R_0$. Thus, for larger R_γ the geometry of the vesicles exposed to low c_{ex} remains unchanged and R_{sp} stays constant. For $W_{LJ} = 4000 T/R_0^2$ the value of R_{sp} increases with R_γ over the whole range. However, vesicles exposed to high

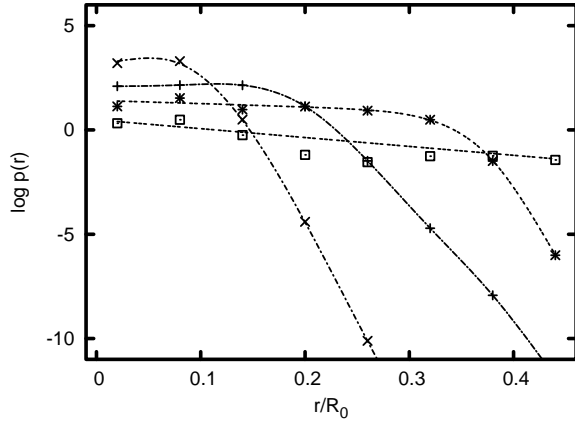


Fig. 8. Probability density $p(x, y) = p(r)$ for finding the projection of the vesicle's center of mass onto the substrate at a distance $r = \sqrt{x^2 + y^2}$ from the center of an attractive circular domain with radius $R_\gamma = 0.5 R_0$ (+), $R_\gamma = 0.9 R_0$ (x), $R_\gamma = 1.3 R_0$ (*), and $R_\gamma = 1.7 R_0$ (□). Results are shown for potential strength $W_{LJ} = 2000 T/R_0^2$ and bending rigidity $\kappa = 15 T$. The length R_0 is defined via the vesicle surface area $A = 4\pi R_0^2$. Osmotic effects are excluded. Lines are intended to guide the eye.

c_{ex} concentrations and low volume adapt more flexible to large domain radii $R_\gamma \approx 1.1 R_0$ so that the order is reversed and vesicles exposed to the lowest c_{ex} have the largest spherical radius R_{sp} .

Lateral localization of adhering vesicles

In the last paragraph, we have investigated the shapes of fluid vesicles which adhere to an attractive circular domain. Such a setup may be used to fix the lateral position of an adhering vesicle. Returning to vesicles composed of lipid bilayers with typical bending rigidities $\kappa = 10\text{--}15 T$, we investigate how much the center of mass of an adhering vesicle can be localized by a circular attractive domain. Therefore, we analyze the fluctuations of the center of mass of an adhering vesicle which provides information for finding the center of mass at a certain position.

Let $p(x, y)$ denote the probability density for finding the center of mass of the vesicle interior at a given x - and y -coordinate. The z -coordinate characterizes its distance from the substrate. Since the considered physical system is axially symmetric with respect to the center of the attractive circular domain, the probability density $p(x, y)$ depends only on the distance of the vesicle center $r \equiv \sqrt{x^2 + y^2}$ from the center of the domain, *i.e.*,

$$p(x, y) = p(r) \quad (10)$$

and can be easily calculated from the probability density $\tilde{p}(r)$ for finding the vesicle's center at *any* place with distance r from the center of the domain via

$$p(r) = \frac{\tilde{p}(r)}{2\pi r}. \quad (11)$$

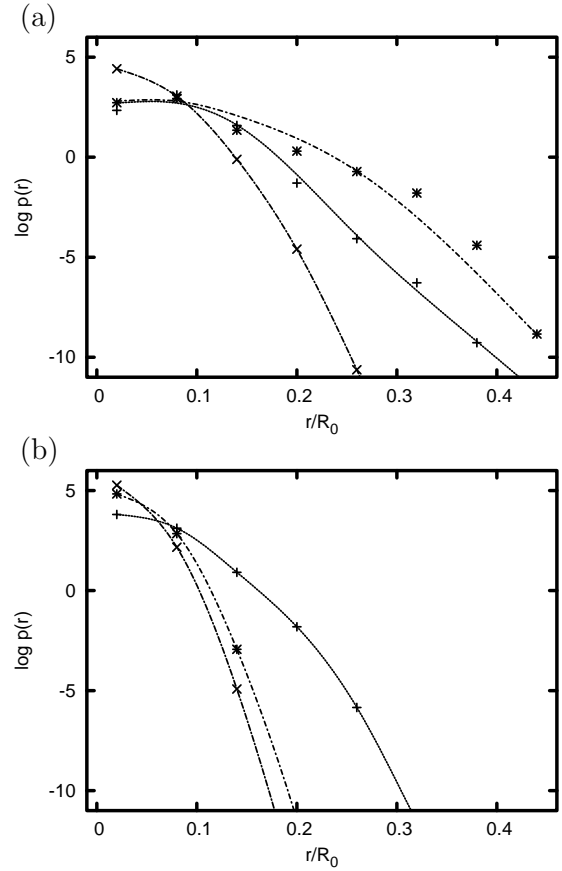


Fig. 9. Probability density $p(x, y) = p(r)$ for finding the projection of the vesicle's center of mass onto the substrate at a distance $r = \sqrt{x^2 + y^2}$ from the center of an attractive circular domain as in Figure 8 but with (a) altered bending rigidity $\kappa = 10 T$, $W_{LJ} = 2000 T/R_0^2$ and (b) altered potential strength $W_{LJ} = 4000 T/R_0^2$, $\kappa = 15 T$. Results are shown for domain radii $R_\gamma = 0.5 R_0$ (+), $R_\gamma = 0.9 R_0$ (x), and $R_\gamma = 1.3 R_0$ (*).

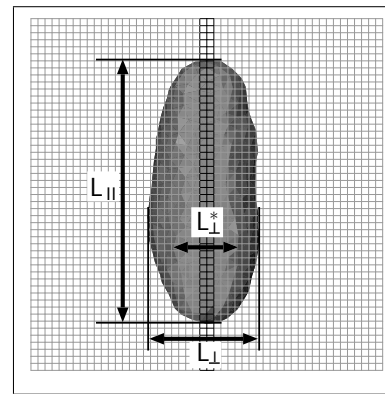


Fig. 10. Characteristic configuration of a vesicle adhering to an attractive stripe on a planar substrate. Arrows indicate the maximum extension of the vesicle perpendicular to the stripe L_{\perp} , the maximum extension of the contact area perpendicular to the stripe L_{\perp}^* , and the length of the vesicle parallel to the stripe L_{\parallel} .

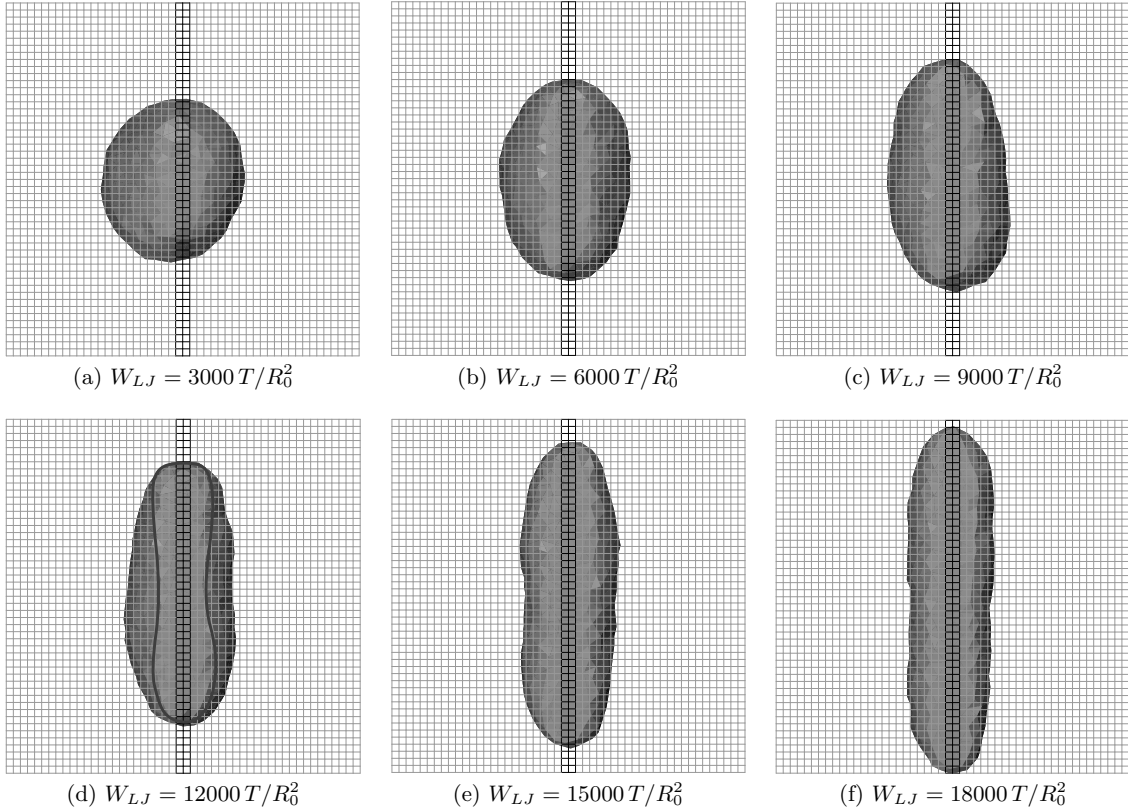


Fig. 11. Typical configurations of an adhering vesicle with bending rigidity $\kappa = 20 T$ to an attractive stripe of width $L_\gamma = 0.3 R_0$. The strength of the attractive potential varies between $W_{LJ} = 3000 T/R_0^2$ and $W_{LJ} = 18000 T/R_0^2$. In panel (d), the contact line (dark solid line) attains a shape that is constricted in the middle.

With the help of a sampling scheme for probability distributions that we introduced in [23], we calculated $p(r)$ for various values of the bending rigidity, the domain radius, and the strength of its attractive potential, see Figures 8 and 9. The results indicate that there is an optimal domain radius of about

$$R_\gamma \simeq 0.9 R_0, \quad (12)$$

which maximizes the probability $p(r)$ for small r and provides the optimum lateral localization of the center of mass above the attractive domain. Smaller domain sizes localize the vesicle's contact area close to the domain while the rest of the membrane and, in particular, the center of mass strongly fluctuates. For large values $R_\gamma \gtrsim 0.9 R_0$, the attractive domain is larger than the contact area so that the vesicle can move laterally until it reaches the domain boundary. Thus, the strength of localization of the whole vesicle is reduced.

4 Adhesion to an attractive stripe-shaped domain

The shape of a fluid vesicle adhering to an attractive stripe-shaped domain with coordinates $-\frac{L_\gamma}{2} \leq x \leq \frac{L_\gamma}{2}$ at

the planar substrate can be characterized by the following geometrical quantities:

- L_\parallel , the maximum extension of the vesicle parallel to the stripe.
- L_\perp , the maximum extension of the vesicle perpendicular to the stripe.
- L_\perp^* , the maximum extension perpendicular to the stripe for the membrane part which is closer to the substrate than a distance $z \leq \ell/4$, where ℓ is the average tether length of the tethered-beads model.

Examples of L_\parallel , L_\perp , and L_\perp^* are shown in Figure 10 for a characteristic vesicle configuration. During the simulations, thermal averages $\langle L_\parallel \rangle$, $\langle L_\perp \rangle$, and $\langle L_\perp^* \rangle$ are calculated from instantaneous values of L_\parallel , L_\perp , and L_\perp^* , which are extracted from vesicle configurations on a regular basis. The quantity $\langle L_\perp^* \rangle$ is basically the average width of the contact area.

We found the following types of vesicle shapes in our simulations. For very small potential depths W_{LJ} , the vesicle has an almost spherical shape in contact with the attractive stripe (Fig. 11(a)). The shape becomes bulge like with increasing W_{LJ} and, finally, changes into a membrane tube with hemispheres on both ends. Such configurations are shown in Figures 11(b–f). For large bending rigidities and narrow stripes, there are intermediate

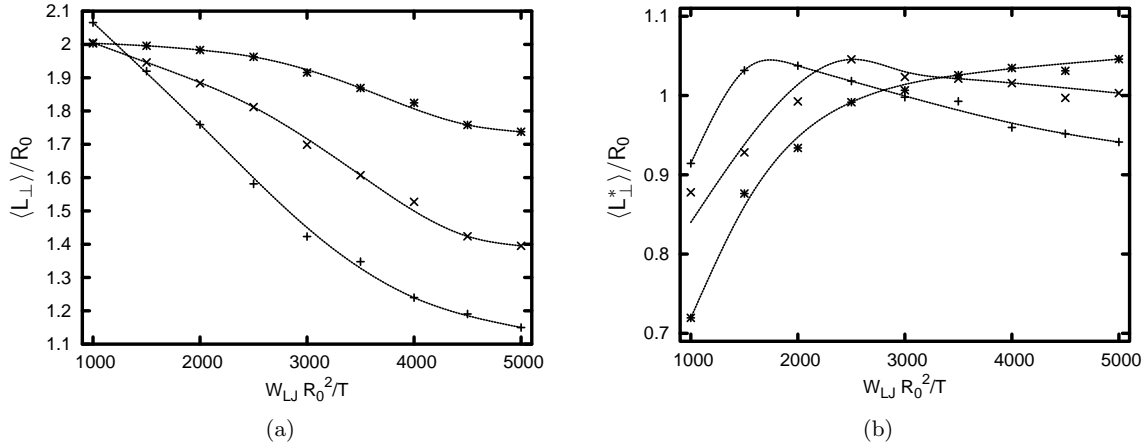


Fig. 12. Thermal averages of (a) the total width $\langle L_{\perp} \rangle$ of the vesicle perpendicular to the stripe and (b) the width $\langle L_{\perp}^* \rangle$ of the contact zone of the vesicle in units of the reference length R_0 as function of the reduced strength $W_{LJ} R_0^2 / T$ of the attractive potential of the stripe with width $L_{\gamma} = 0.7 R_0$. The bending rigidity of the vesicle membrane has been set to $\kappa = 5T$ (+), $\kappa = 10T$ (x), and $\kappa = 20T$ (*). The length R_0 is defined via the vesicle surface area $A = 4\pi R_0^2$. Lines are intended to guide the eye.

configurations with a contact line shape that is constricted in the middle (Fig. 11(d)).

The geometry of the vesicle adhering to the attractive stripe was analyzed with Monte Carlo simulations as a function of W_{LJ} and κ . An increasing potential strength W_{LJ} results in an increasing thermal average $\langle L_{\parallel} \rangle$ of the vesicle extension parallel to the stripe in combination with a decreasing thermal average $\langle L_{\perp} \rangle$ of the maximum extension perpendicular to the stripe. The same shape change occurs if the bending rigidity κ is decreased. However, the thermal average of the contact area extension $\langle L_{\perp}^* \rangle$ perpendicular to the stripe shows a non-monotonic dependence on W_{LJ} . Plots of $\langle L_{\perp} \rangle$ and $\langle L_{\perp}^* \rangle$ are shown in Figure 12 as a function of the reduced adhesion strength of the stripe.

The non-monotonic behavior of $\langle L_{\perp}^* \rangle$ as a function of W_{LJ} is an immediate result of the vesicle's closed topology. At low values of W_{LJ} , the vesicle is almost spherical. With increasing potential strength, the vesicle is more strongly bound and the contact zone expands in all directions. At larger values of W_{LJ} , the width of the contact zone perpendicular to the stripe is reduced in favor of an expansion along the stripe.

5 Conclusion

In this article, we have shown that, in addition to the osmotic conditions inside and outside the vesicle membrane and the geometry and strength of the attractive γ domain, fluctuations of the vesicle membrane can strongly influence the adhesion behavior of fluid vesicles to chemically structured substrates. If the whole attractive γ domain is covered by the contact area of the vesicle, further deflation of the vesicle lowers the membrane tension. If the bending rigidity is low, the membrane shows strong fluctuations around an average shape. For an attractive circular domain, this shape is approximately a spherical

cap, corresponding with the shape of an adhering drop or the shape of adhering vesicles in the high-tension regime. Larger bending rigidities yield smoother shapes which deviate clearly from a spherical-cap geometry.

For small bending rigidities, the qualitative behavior of the projected contact area depends on the radius R_{γ} of the attractive domain. While for large R_{γ} it increases with increasing exterior concentration c_{ex} of osmotically active particles, it shrinks with increasing c_{ex} for small radii R_{γ} . A similar behavior is found for the spherical radius R_{sp} of the average spherical cap shape.

The localization of a fluid vesicle at a predefined position on a planar substrate can be achieved by means of chemically structuring the substrate surface. With an attractive circular domain on the substrate, our simulations show for various values of W_{LJ} and κ that the strongest localization of the vesicle is achieved by a domain radius of $R_{\gamma} \simeq 0.9 R_0$. Smaller as well as larger domain radii distinctly reduce the localization strength.

For vesicles adhering to an attractive stripe, we investigated characteristic properties of the shape like L_{\perp}^* , the maximum extension of the contact area perpendicular to the stripe. The thermal average $\langle L_{\perp}^* \rangle$ changes non-monotonically with the adhesion strength.

Appendix A. A deflated vesicle adhering to an attractive circular domain

In the following, a simple model is derived for a vesicle with low bending rigidity adhering to an attractive circular domain. We consider a deflated vesicle whose non-adhering membrane region undergoes strong fluctuations. The following considerations rationalize that the membrane fluctuates around an average surface with the shape of a spherical cap. Related to the area of the average surface, a tension can be defined which vanishes with

increasing external concentration. Our approach is based on the following assumptions:

- The reduced bending rigidity κ/T is small.
- Due to the adhesion potential the fluctuations in the contact zone are strongly reduced. In comparison with the oscillations of the non-adhering membrane, the adhered membrane is rather flat and the intrinsic membrane area in the contact zone can be approximated by $A^* \simeq A_p^* \simeq \pi R_\gamma^2$ (compare configurations in Fig. 3).
- The non-adhering intrinsic membrane surface S_{na} with the intrinsic area $A_{na} = A - A^*$ is fluctuating around a constant average shape S_{av} with an area A_{av} . Here, A_{av} does not include the adhesion area A^* , which implies $A^* + A_{av} \leq A$.
- The bending energy of the average shape S_{av} is small in comparison with that of the strongly fluctuating shape S_{na} of the intrinsic membrane.
- The amplitudes of the fluctuations around S_{av} are small compared to R_0 .
- The volume V inside the vesicle is independent of the fluctuations of S_{in} , so that the osmotic energy E_{osm} is determined by the average shape S_{av} .
- The fluctuations of the intrinsic surface S_{na} around the smooth average surface S_{av} can be determined from those of a membrane with intrinsic area A_{in} on a flat area of size A_{av} .

With these assumptions we can determine the optimum average shape S_{av} for the non-adhering membrane S_{na} with fixed intrinsic area A_{na} . The free energy of the system is given by

$$F = F_{fl} + E_{osm} + E_{ad}, \quad (\text{A.1})$$

where the adhesion energy is roughly constant and F_{fl} includes the bending energy and the entropy due to the membrane fluctuations. It can be written as

$$F_{fl}(A_{av}) = -T \ln(Z_{fl}) \quad (\text{A.2})$$

with

$$Z_{fl} = \int d\{h\} \delta(A[\{h\}] - A_{na}) \exp(-E_{el}[\{h\}]/T), \quad (\text{A.3})$$

where $\{h\}$ is the set of local fluctuation amplitudes. According to our assumptions, F_{fl} is independent of the osmotic energy. The integral in equation (A.3) can be calculated by a Fourier transformation. Analogously to the approach presented by Fournier and coworkers [35], we find:

$$F_{fl}(A_{av}) = \frac{TA_{av}\Lambda^2}{8\pi} \left(\left((\pi R_0 \Lambda)^{-2} - 1 \right) \ln(q-1) + \ln(q) \right) \quad (\text{A.4})$$

with

$$q = \exp \left(8\pi \frac{\kappa}{T} \frac{A_{na} - A_{av}}{A_{av}} \right). \quad (\text{A.5})$$

Λ is the largest wave number of the fluctuations, typically determined by the membrane thickness. The smallest wave number is set to $(\pi R_0)^{-1}$. If R_0 , Λ , N , c_{ex} , κ , T and A is fixed, $F = F_{fl}(A_{av}) + E_{osm}(V) + \text{const}$ is a function of

V and A_{av} . For fixed V , the optimum A_{av} is given by the minimum of $F_{fl}(A_{av})$. However, for small enough

$$\frac{\kappa}{T} < \frac{1}{4\pi} \frac{A_{av}}{A_{na} - A_{av}} \ln(\pi R_0 \Lambda), \quad (\text{A.6})$$

the derivative

$$\left(\frac{dF}{dA_{av}} \right)_V$$

is always positive so that F_{fl} is minimized by the smallest possible area A_{av} . In our case, the smallest average area for a given volume V is provided by a spherical-cap geometry with an area $A_{av} =: A_{sp}(V)$.

For a spherical cap with a given flat area of radius R_γ , there is a unique relation between V and A_{sp} , namely

$$V = \frac{\pi}{6} \sqrt{\frac{A_{sp}}{\pi} - R_\gamma^2} \left(\frac{A_{sp}}{\pi} - R_\gamma^2 \right). \quad (\text{A.7})$$

Hence, the shape of the average surface S_{av} is determined by

$$\frac{dF_{fl}(A_{sp})}{dA_{sp}} \frac{dA_{sp}(V)}{dV} + \frac{dE_{osm}(V)}{dV} = 0. \quad (\text{A.8})$$

With the mean curvature M of the spherical cap, one has

$$\frac{dA_{sp}(V)}{dV} = \frac{M}{2}. \quad (\text{A.9})$$

If we define a tension $\Sigma_{sp} \equiv \frac{dF_{fl}(A_{sp})}{dA_{sp}}$ with respect to the spherical-cap area A_{sp} , equation (A.8) becomes the Laplace equation, as expected:

$$\Sigma_{sp} \frac{M}{2} = P_{os}. \quad (\text{A.10})$$

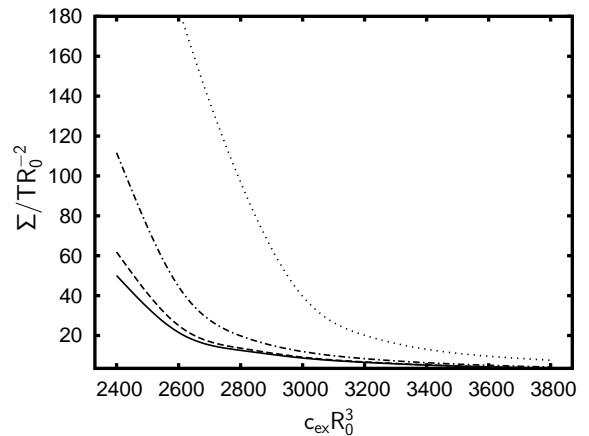


Fig. 13. Reduced tension $\Sigma_{sp} R_0^2/T$ of a deflated vesicle as a function of the reduced external concentration $c_{ex} R_0^3$. The vesicle is adhering to a strongly adhesive circular domain with radius $R_\gamma = 0.5$ (solid line), $R_\gamma = 0.7$ (dashed line), $R_\gamma = 0.9$ (dash-dotted line), and $R_\gamma = 1.1$ (dotted line). The curves show results from the analytic approach described in the appendix.

With $\Delta A \equiv A_{na} - A_{sp}(\Sigma_{sp})$, one has

$$\ln \left(\frac{\Sigma_{sp}/\kappa + \Lambda^2}{\Sigma_{sp}/\kappa + (\pi R_0)^{-2}} \right) = 8\pi\kappa \frac{\Delta A}{A_{sp}} + O \left(\left(\frac{\Delta A}{A_{na}} \right)^2 \right), \quad (\text{A.11})$$

which corresponds to the expression for $\Delta A(\Sigma)$ in equation (A.7) of [36], if terms of the order $(\Delta A/A_{na})^2$ can be neglected. By solving equation (A.10), the tension Σ_{sp} can be determined as a function of the adhesion zone radius R_γ and the external concentration c_{ex} . Results for $\kappa = 0.1T$ are shown in Figure 13.

References

1. D.T. Chiu, C.F. Wilson *et al.*, *Science* **283**, 1892 (1999).
2. D.P. Nikolelis, T. Hianik, U.J. Krull, *Elektroanal.* **11**, 7 (1999).
3. P. Fromherz, V. Kiessling, K. Kottig, G. Zeck, *Appl. Phys. A* **69**, 571 (1999).
4. M. Karlsson, M. Davidson, R. Karlsson, A. Karlsson, J. Bergenholtz, Z. Konkoli, A. Jesorka, T. Lobovkina, J. Hurtig, M. Voinova, O. Orwar, *Annu. Rev. Phys. Chem.* **55**, 613 (2004).
5. N. Kohli, S. Vaidya, R.Y. Ofoli, R.M. Worden, I. Lee, *J. Colloid Interface Sci.* **301**, 461 (2006).
6. J.T. Groves, N. Ulman, Paul S. Cremer, S.G. Boxer, *Langmuir* **14**, 3347 (1998).
7. K.A. Burrridge, M.A. Figa, J.Y. Wong, *Langmuir* **20**, 10252 (2004).
8. A.-L. Bernard, M.-A. Guedeau-Boudeville, O. Sandre, S. Palacin, J.-M. di Meglio, L. Jullien, *Langmuir* **16**, 6801 (2000).
9. N. Patrino, C. McCague, P.R. Norton, N.O. Peterson, *Langmuir* **23**, 715 (2007).
10. H.S. Jung, J.M. Kim, J.W. Park, S.E. Lee, H.Y. Lee, R. Kuboi, T. Kawai, *J. Biosci. Bioeng.* **102**, 28 (2006).
11. U. Seifert, R. Lipowsky, *Phys. Rev. A* **42**, 4768 (1990).
12. U. Seifert, K. Berndl, R. Lipowsky, *Phys. Rev. A* **44**, 1182 (1991).
13. E.M. Blokhuis, W.F.C. Sager, *J. Chem. Phys.* **110**, 3148 (1999).
14. C. Tordeux, J.-B. Fournier, P. Galatola, *Phys. Rev. E* **65**, 041912 (2002).
15. R. Capovilla, J. Guven, *Phys. Rev. E* **66**, 041604 (2002).
16. A.-L. Bernard, M.-A. Guedeau-Boudeville, L. Julien, J.-M. di Meglio, *Langmuir* **16**, 6809 (2000).
17. A. Boulbitch, Z. Guttenberg, E. Sackmann, *Biophys. J.* **81**, 2743 (2001).
18. P.-G. de Gennes, P.-H. Puech, F. Brochard-Wyart, *Langmuir* **19**, 7112 (2003).
19. F. Brochard-Wyart, P.-G. de Gennes, *C. R. Phys.* **4**, 281 (2003).
20. A.-S. Smith, U. Seifert, *Langmuir* **21**, 11357 (2005).
21. I. Durand, P. Jönson, C. Misbah, A. Valance, K. Kassner, *Phys. Rev. E* **56**, R3776 (1997).
22. J. Solon, P. Streicher, R. Richter, F. Brochard-Wyart, P. Bassereau, *Proc. Natl. Acad. Sci. U.S.A.* **103**, 12382 (2006).
23. G.T. Linke, R. Lipowsky, T. Gruhn, *Phys. Rev. E* **71**, 051602 (2005).
24. U. Seifert, *Phys. Rev. Lett.* **74**, 5060 (1995).
25. A. Baumgärtner, S.M. Bhattacharjee, *J. Chem. Phys.* **107**, 4390 (1997).
26. T. Gruhn, R. Lipowsky, *Phys. Rev. E* **71**, 011903 (2005).
27. T. Gruhn, T. Franke, R. Dimova, R. Lipowsky, *Langmuir* **23**, 5423 (2007).
28. R. Lipowsky, M. Brinkmann, R. Dimova, T. Franke, J. Kierfeld, X. Zhang, *J. Phys.: Condens. Matter* **17**, S537 (2005).
29. P.B. Canham, *J. Theor. Biol.* **26**, 61 (1970).
30. W. Helfrich, *Z. Naturforsch.* **28c**, 693 (1973).
31. N. Metropolis, A.W. Rosenbluth, M.N. Rosenbluth, A.H. Teller, E. Teller, *J. Chem. Phys.* **21**, 1087 (1953).
32. D.M. Kroll, G. Gompper, *Science* **255**, 968 (1992).
33. E. Evans, W. Rawicz, *Phys. Rev. Lett.* **64**, 2094 (1990).
34. B.A. Coldren, H. Warriner, R. van Zanten, J.A. Zasadzinski, E.B. Sirota, *Proc. Natl. Acad. Sci. U.S.A.* **103**, 2524 (2006).
35. J.-B. Fournier, A. Ajdari, L. Peliti, *Phys. Rev. Lett.* **86**, 4970 (2001).
36. R. Lipowsky, *J. Phys. II* **2**, 1825 (1992).